Research Square

Preprints are preliminary reports that have not undergone peer review.
They should not be considered conclusive, used to inform clinical practice,
or referenced by the media as validated information.

Phase-matched ion pre-acceleration by upstreammagnetic dipole vortices in relativistic collisionlessshocks

Neda Naseri

nnaseri@adelphi.edu

Adelphi University

Hava Turkakin

Utica College

Gennady Shvets

Cornell University

Article

Keywords:

Posted Date: September 15th, 2026

DOI: https://doi.org/10.21203/rs.3.rs-10767397/v1

License: This work is licensed under a Creative Commons Attribution 4.0 International License.
Read Full License

Additional Declarations: No competing interests reported.

Version of Record: A version of this preprint was published at Scientific Reports on October 29th, 2026.
See the published version at https://doi.org/10.1038/s41598-026-77217-x.

Phase-matched ion pre-acceleration by upstream magnetic dipole vortices in relativistic collisionless shocks

Neda Naseri[1,*], Hava Turkakin[2], and Gennady Shvets[3]

[1]Department of Physics, Adelphi University, 1 South Ave, Garden City, New York, USA
[2]Department of Physics, Utica University, Utica, New York, USA
[3]School of Applied and Engineering Physics, Cornell University, Ithaca, New York, 14850, USA
[*]nnaseri@adelphi.edu

ABSTRACT

Collisionless shocks are among the most efficient particle accelerators in the Universe, yet the physical mechanism responsible for energetic upstream seed ions remains poorly understood. Using two-dimensional particle-in-cell simulations of unmagnetized relativistic electron-ion shocks, we investigate ion pre-acceleration by self-generated magnetic dipole vortices (MDVs) in the upstream region of the shock. We identify two distinct ion populations: one remains phase-matched with the moving MDV, undergoes considerable energization, and returns toward the shock, whereas the other escapes upstream after gaining only modest energy. We show that the magnetic component of the Lorentz force reduces the ion's longitudinal velocity relative to the moving MDV, extending the interaction time and allowing the transverse electric field to perform sustained positive work. Decomposition of the electric field shows that both the motional electric field associated with the moving MDV and plasma-generated fields contribute to the observed ion energization. Repeated interactions with successive MDVs can increase ion energy before the particles return to the shock transition region. These results identify upstream MDVs as a self-consistent pre-injection mechanism, providing the energetic seed ions required for subsequent shock acceleration.

Introduction

Collisionless shocks are considered among the most efficient particle accelerators in the Universe and are believed to be responsible for producing energetic particles in environments such as supernova remnants, gamma-ray bursts, pulsar wind nebulae, and relativistic jets. Observations of high-energy radiation, cosmic rays (CRs), and gamma-ray bursts (GRBs) provide evidence for nonthermal particle acceleration associated with collisionless shocks[1–3]. In these plasmas, conversion of bulk-flow energy into energetic particles is mediated entirely by collective electromagnetic processes generated within the shock structure. Therefore, understanding how particles are initially energized before entering subsequent acceleration stages remains one of the central problems in collisionless shock physics.

Collisionless shocks are believed to be mediated by Weibel instability, which leads to fast growth of magnetic field at small scales, plasma isotropization and particle energization at later times[4–11]. A first phase of magnetic field amplification due to Weibel instability happens in the shock front region[11–14]. A simultaneous stage of magnetic field growth occurs due to development of Weibel instability driven by particles moving ahead of shock front, i.e, counter streams, and the incoming cold plasma streams. Counter stream particle flows are particles that are either reflected off shock transition region or escaped interaction with shock transition region. Recent advances in high-power laser experiments have also advanced laboratory studies of collisionless-shock formation under conditions relevant to high-energy astrophysical plasmas. Experiments and supporting kinetic simulations have demonstrated the development of Weibel-mediated collisionless shocks, providing laboratory evidence for the generation of strong magnetic fields and filamentary structures by plasma instabilities[15,16]. These studies highlight the importance of self-generated upstream electromagnetic structures in controlling shock formation and particle dynamics.

In our previous work, we demonstrated that MDVs can emerge self-consistently in the upstream of electron/ion collisionless shocks with no external magnetic field[17]. Similar magnetic structures have been reported in multiple independent studies using different numerical codes and setups[18–20]. The early stage of the interaction involves the generation of quasi-linear elongated MDVs, which subsequently merge to form circularly shaped MDVs. Localized regions of strong magnetic field in the form of magnetic dipole vortices upstream of the shock were observed in the simulations developed during the nonlinear evolution of the electron and ion filaments. MDVs emerge during the stage in which flow energy transformation into thermal energy takes place[17]. The magnetic and electric fields of the MDVs grow, while their longitudinal sizes shrink as they propagate toward the shock front. Building upon these findings, our subsequent study revealed that these self-generated upstream MDVs efficiently

accelerate electrons before they reach the shock transition region. Electron energization was shown to arise from interactions with the electromagnetic fields associated with the evolving MDVs, generating energetic electrons that may later participate in additional acceleration at the shock[21]. The focus of this study is the ion pre-energization mechanism associated with interaction with self-generated MDVs in the upstream of relativistic collisionless electron/ion shocks with no external magnetic field.
Ion acceleration has been extensively investigated in magnetized relativistic collisionless shocks, where shock geometry and the background magnetic field strongly affect particle injection and subsequent acceleration[22,23]. In initially unmagnetized electron–ion shocks, however, the upstream magnetic structure is generated self-consistently by plasma instabilities. Although Weibel-generated turbulence is known to mediate shock formation, how ions can be pre-accelerated within this self-generated upstream environment before reaching the shock transition remains less well understood. Unlike electrons, ions have much larger masses and gyroradii. Consequently, whether propagating MDVs can efficiently pre-accelerate ions, and if so, what electromagnetic processes are responsible, remains unknown. Since magnetic fields alone cannot perform work on charged particles, identifying the physical mechanism responsible for ion pre-acceleration in the upstream region is a central question. Understanding the origin of energetic upstream ions is important because such particles can provide a seed population for subsequent shock acceleration. Particle tracking in unmagnetized relativistic electron–ion shocks has shown that ions can undergo Fermi-like energization through repeated interactions with the shock-generated electromagnetic structures[24].

In this work, we investigate ion pre-acceleration in the upstream region of an unmagnetized relativistic electron-ion collisionless shock using two-dimensional particle-in-cell simulations. We identify two distinct Populations of pre-accelerated ions in the upstream region. By tracking a large number of ions, we identify the physical mechanism responsible for upstream ion pre-acceleration and determine the source of the electric field responsible for the observed energy gain. We identify a self-consistent mechanism for upstream ion pre-acceleration in which MDVs first reduce the ion's longitudinal velocity, maintaining phase matching condition and allowing the electric field to perform positive work. Repeated interactions with multiple MDVs may produce energetic seed ions in a step-by-step manner for subsequent shock acceleration.

Because of the periodic formation of MDVs in the upstream region of the shock, an ion may interact with multiple MDVs before reaching the shock transition region. Such repeated interactions with MDVs may boost its energy, making the understanding of a single MDV interaction the essential first step toward describing upstream ion injection. We investigate ion energization from the scale of a single MDV interaction to the broader role of repeated interactions throughout the shock upstream region. The ion pre-acceleration identified here has broader implications for collisionless-shock acceleration. By generating an energetic ion Population upstream of the shock, MDVs effectively supply a Population of seed particles that are more efficiently injected into subsequent acceleration processes at the shock, including repeated shock crossings. Understanding the production of these seed ions is therefore an important step toward a comprehensive description of particle acceleration in relativistic collisionless shocks.

Together with our previous investigation of electron pre-acceleration, the present work establishes self-generated upstream MDVs as efficient pre-acceleration regions for both plasma species. More broadly, the results suggest that repeated interactions with propagating MDVs may prepare particles for subsequent acceleration at relativistic collisionless shocks.

Results

Simulation set-up

The two-dimensional (2D) version of the relativistic parallel particle-in-cell (PIC) code VLPL is used[25]. The code was modified to minimize noise properties of numerical instabilities, by using third-order shaped particles and current smoothing. A rectangular simulation box in the $x-z$ plane with the dimensions $L_x = 1300\, l_{pe}$ and $L_z = 130\, l_{pe}$ and the grid sizes $\Delta z = l_{pe}/10$ and $\Delta x = l_{pe}/10$ is used. Here $l_{pe} = c/\omega_{pe}$ is the electron inertial length, that is the typical transverse spatial scale of the filaments, $\omega_{pe} = \sqrt{\frac{4\pi n_0 e^2}{\gamma_0 m_e}}$ is the electron plasma frequency, γ_0 is the relativistic gamma factor of incoming plasma flow, e and m_e denote the charge and mass of electron, and n_0 is the unperturbed density of electrons. Periodic boundary conditions are applied for particles and fields in the transverse (z) direction. The left boundary is reflecting for particles and fields. The simulation is terminated when counter-streaming particles reach the right boundary of the simulation domain. Therefore, no particle leaves the domain during simulation. Fresh flow of electrons and ions enter the domain continuously from the right boundary. Each computational cell is initialized with 16 macro-particles: 8 electrons and 8 ions. We assume that initially the electron-ion (e,i) plasma beam with the mass ratio $m_i/m_e = 32$ and equal charges $q_i = q_e$, equal densities n_0, and relativistic velocities v_x (corresponding to $\gamma_0 \equiv 1/\sqrt{1 - v_x^2/c^2} = 15$) moves to the left (in the direction opposite to x-axis direction). To reduce computational effort, the initial contact point of the two counter-propagating streams is modeled as a reflecting wall at $x = 0$[11]. The simulation is performed in the reflecting wall frame, where the downstream (thermalized) plasma behind the shock has a vanishing average flow velocity. All densities (electron and ion) and fields (electric and magnetic) are expressed in dimensionless units as $\tilde{N}_{i,e} = n_{i,e}/n_0$, $\tilde{B}_y = eB_y/m_e\omega_{pe}c\sqrt{\gamma_0}$, and $\tilde{E}_{x,z} = eE_{x,z}/m_e\omega_{pe}c\sqrt{\gamma_0}$.

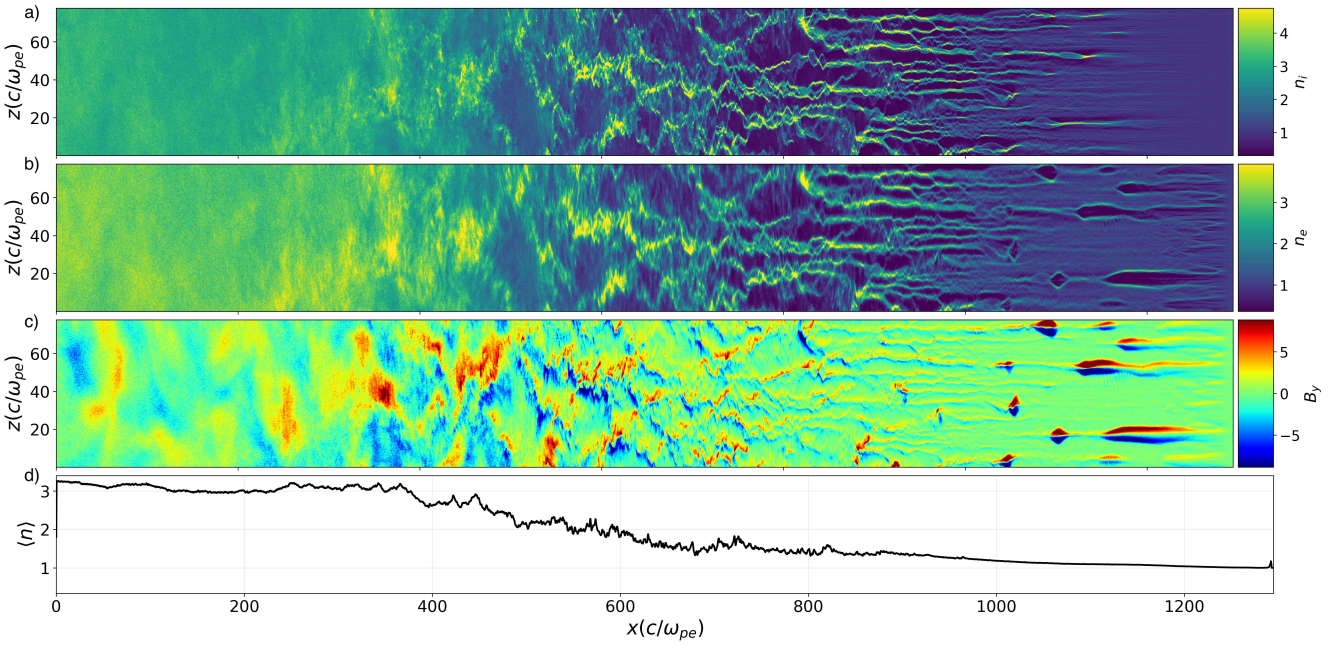


Figure 1. (a,b) Color plots of normalized ion and electron density and (c) normaized out of plane magnetic field (B_y) in $x-z$ plane at $\omega_{pe}t = 1140$. (d) transversely averaged plasma density normalized to upstream unperturbed density.

Formation and Evolution of Upstream Magnetic Dipole Vortices (MDVs)

The structure of the fully formed shock at $\omega_{pe}t = 1140$ is shown in Fig. 1. Figure 1 (a,b) show the colorplots of the normalized electron and ion densities, respectively. Figure 1(c) shows the color plot of out of plane magnetic field (B_y). The transversely averaged plasma density $\tilde{n}_(x) = \langle n(x,z)/n_0 \rangle$ ($\langle\rangle$ denotes transverse averaging over the z-dimension) are plotted in Fig.1 (d) that was chosen to represent a fully developed shock.

Our focus is on the upstream region of the shock, where the incoming cold streams interact with isotropized counter stream flow. The upstream region of the relativistic collisionless shock is dominated by the so-called counter stream particles, incoming flow of particles interacting with lower density stream of isotropized counter stream electrons and relatively cold counter stream ions, that already escaped the shock region or were never trapped. Here we summarize MDV generation and evolution in the upstream. In overlapping region the incoming cold streams of electrons and ions meet with counter stream isotropized electrons and ions with considerable thermal spread. The interaction of counter stream flows with cold incoming flow leads to electron Weibel instability. Electron Weibel instability initiates quickly as the incoming and counter streams meet in the overlapping region. The growth rate of electron Weibel instability is found to be 0.13 ω_{pe} that is significantly less than for the cold beam plasma case $\delta_e = \sqrt{2}\ \omega_{pe}$, and in agreement with the estimate for a hot electron beam $\simeq \delta_e(1-\Delta\gamma_\perp/\gamma_0)$[6], where $\Delta\gamma_\perp$ is the transverse energy spread and $\Delta\gamma_\perp \backsimeq \gamma_0$. Initially, small-scale filaments are formed, magnetic field grows and then instability saturates. The maximum value of generated magnetic field is in agreement with estimate for saturation level $B_{y,s} \simeq \sqrt{\gamma_0}$[26]. There is no significant charge imbalance in filaments as electron Weibel instability saturates in the overlapping region, where the counter stream Population meets cold flow[17]. At the final stage of electron Weibel instability, the electrons in incoming beam are considerably isotropic. The ion Weibel instability is later developed in the background of well-thermalized electrons. The growth rate of ion Weibel instability is found to be close to 0.34 ω_{pi}, (here, $\omega_{pi} = \sqrt{4\pi e^2 n_0/\gamma_0 m_i}$ is the ion plasma frequency) that is less than the estimate for cold approximation ($\delta_i = \sqrt{2}\ \omega_{pi}$)[13], since there is considerable background magnetic field that makes a standard linear analysis not applicable. As the linear stage of the ion Weibel instability terminates, current pinching and filament-neck formation occur. The resulting nonlinear evolution produces elongated localized magnetic vortices that subsequently transform into large-scale magnetic bubbles[17]. The magnetic and electric fields of the MDV grow during propagation towards downstream. The magnetic field of the MDV increases in a non-monotonous manner by a factor of $\approx 5 \sim \sqrt{m_i/m_e}$ with respect to the background magnetic field[17].

Self-generated MDVs move in the plasma density gradient direction toward the shock front[27]. Our simulations show that the axial velocity of the magnetic vortices increases as they move along the density gradient. The drift velocity of magnetic vortices, propagating in a plasma with a density gradient, is estimated to be $v_{d,x}/c \approx \sqrt{\frac{\alpha B_y^2}{1+\alpha B_y^2}}$[28], where $\alpha = \frac{m_e n_0}{m_i \gamma_0 n}$; here, n is

the ion density. The longitudinal drift velocity of the magnetic vortices during evolution observed in simulations increases from $|v_x/c| \approx 0.2$ to 0.5 (when the ion density increases from n_0 to $\approx 1.5n_0$, and B_y increases from 3.1 to 15) in agreement with the observed MDV velocities in our simulations.

Ion Energization in uptream region

During the growth phase of MDVs, both electrons and ions experience energization. Electrons respond to the electromagnetic (EM) fields generated by the evolving MDVs immediately upon their formation, while ion acceleration occurs only when ions interact with the nonlinear stage of the MDVs, where the EM fields reach their maximum. To identify the mechanism of ion acceleration, we tracked a large number of energized ions interacting with MDVs in the upstream region. Two characteristic trajectories were selected: one ion that reversed its direction and returned toward the shock (Population I), and another that continued propagating upstream after leaving the MDV (Population II). These trajectories illustrate the two dominant groups of ions observed in the simulation. The two ion Populations show different dynamical behavior and energy gain. Population II ions experience smaller energy gains, whereas Population I ions, which reverse their direction of motion and return toward the shock transition region, undergo much stronger energization. Figure 2 compares the evolution of these sample ions during their interaction with the moving MDV. Panel (a) shows the trajectories overlaid on the transverse electric field E_z. The dynamics of the two ion populations are further illustrated in Supplementary Materials. Both sample ions deflect while crossing the MDV due to the Lorentz force. Population I ion receives a larger kick due to Lorentz force and changes direction and returns towards shock transition region. The Population II ion also deflects but continues moving towards upstream. The corresponding momentum evolution is shown in panels (b) and (c). Before entering the MDV, both ions have similar longitudinal momentum characteristic of the counter stream flow. During the interaction, however, the Population I ion undergoes a significant decrease in longitudinal momentum together with a strong increase in transverse momentum. This momentum evolution shows that the localized electromagnetic fields strongly redirect the ion motion while simultaneously increasing its transverse momentum and total energy. The energy evolution of the two ions is presented in panel (d). For the Population I ion, the energy increases rapidly while the particle stays inside the MDV, leading to an energy increase approximately four times larger than that of the Population II ion.

Mechanism of Longitudinal Slowing and Phase Matching

Sample trajectories in Fig. 2 show that Population I ions experience a much larger decrease in longitudinal momentum than Population II ions. However, the physical mechanism behind this difference is not yet evident. Because only electric fields can perform work on charged particles, the observed decrease in p_x must result from the longitudinal component of the Lorentz force. To identify the dominant mechanism, we calculated the longitudinal electric and magnetic contributions of the Lorentz force. Figure 3(a) compares the longitudinal electric force, $F_{x,E} = qE_x$, the longitudinal magnetic force, $F_{x,B} = -qv_zB_y$, and their sum F_x during the interaction of the sample Population I ion with the MDV. Figure 3 shows that the longitudinal magnetic component of the Lorentz force dominates the longitudinal electric force. Throughout most of the interaction, the magnetic contribution is considerably larger than the electric contribution and closely follows the total longitudinal force. The strongest slowdown occurs while the ion travels the region of maximum magnetic field inside the MDV, indicating that the decrease in longitudinal momentum is governed primarily by the magnetic component of the Lorentz force. Figure 3(b) shows total longitudinal momentum change, Δp_x, compared with the momentum change due to longitudinal electric and magnetic Lorentz forces. The longitudinal momemntum change due to the magnetic component reproduces nearly the entire momentum change, whereas the longitudinal momentum change due to the electric component contributes only a small fraction. This demonstrates that the decrease in longitudinal momentum is almost entirely due to longitudinal magnetic force. These results establish the first step of the ion pre-acceleration mechanism. The magnetic field continuously redirects the particle, reducing its longitudinal velocity relative to the moving MDV. This reduction in longitudinal momentum allows the ion to remain synchronized with the moving structure for a much longer time. As shown in the following section, this extended phase-matched interaction allows the transverse electric field to perform positive work, ultimately resulting in the large energy gains characteristic of Population I ions.

Phase Matching and Ion Energization

The strong decreae of the longitudinal momentum of Population I ions, shown in Fig. 3 changes the motion of the ion relative to the moving MDV. To understand the physical mechanism, we introduce the relative longitudinal coordinate, $\xi(t) = x(t) - x_d(t)$, where $x(t)$ and $x_d(t)$ are the longitudinal positions of the ion and the MDV, respectively. The corresponding relative velocity is $v_{rel,x} = \frac{d\xi}{dt} = v_x - v_{d,x}$, where $v_{d,x}$ is the MDV propagation velocity. The displacement of the ion relative to the MDV after entering the interaction region at t_{entry} is therefore $\Delta\xi(t) = \int_{t_{entry}}^{t}(v_x(t') - v_{d,x}(t'))dt'$. An ion remains within the accelerating region of the MDV as long as its relative displacement does not exceed the characteristic longitudinal extent L_d of that region, $|\Delta\xi(t)| = |\int_{t_{entry}}^{t}(v_x(t') - v_{d,x}(t'))dt'| \lesssim L_d$. Thus, the duration of the interaction depends on the relative velocity $|v_x - v_{d,x}|$.

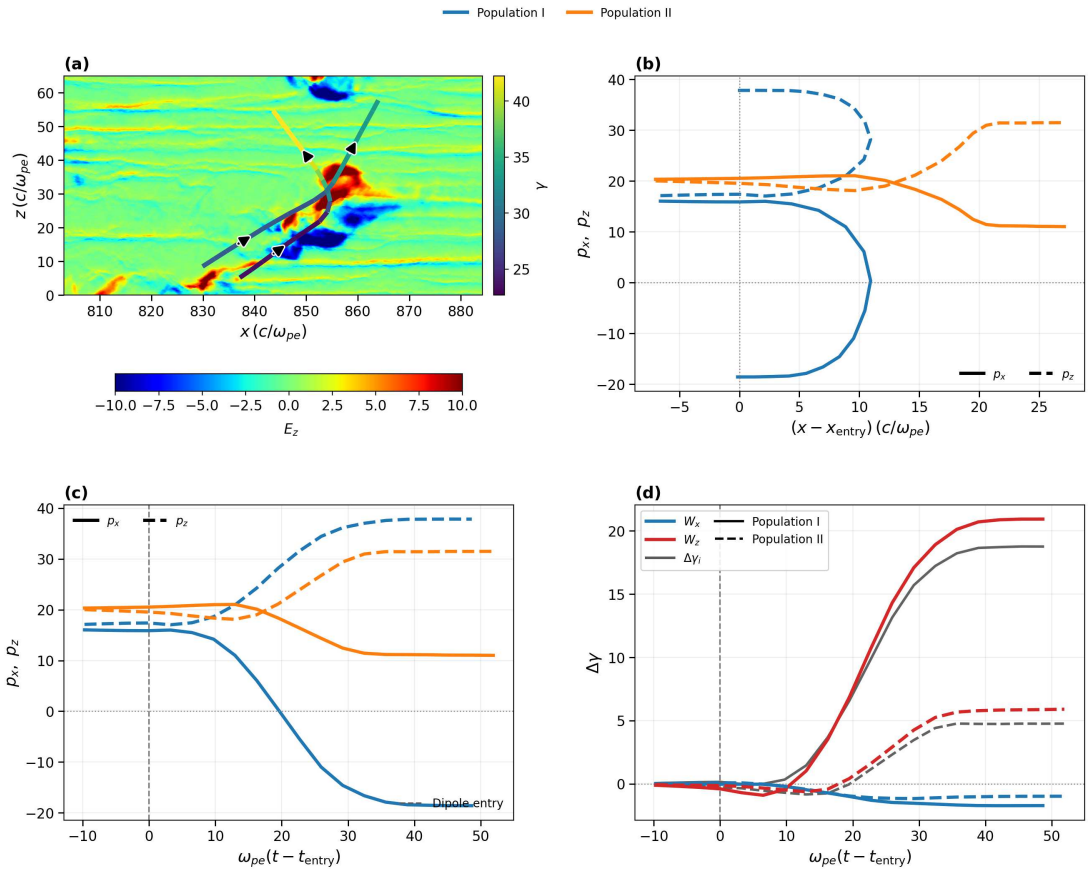


Figure 2. (a) Trajectories of sample Population I (blue) and Population II (orange) ions superimposed on the transverse electric field E_z. The trajectories are color coded by the ion energy, illustrating much larger energization of the Population I ion during its interaction with the MDV. (b) Evolution of the longitudinal (p_x, solid) and transverse (p_z, dashed) momentum as a function of position measured from the dipole-entry location. The Population I ion reverses its longitudinal momentum while gaining a much larger transverse momentum, whereas the Population II ion experiences only a modest momentum change and continues propagating upstream. (c) Evolution of the momentum components as a function of time measured from dipole entry. The gray dashed line marks the instant the ions enter the magnetic dipole. (d) Total longitudinal (W_x, blue) and transverse (W_z, red) work done together with the ion energy gain ($\Delta\gamma$, gray).

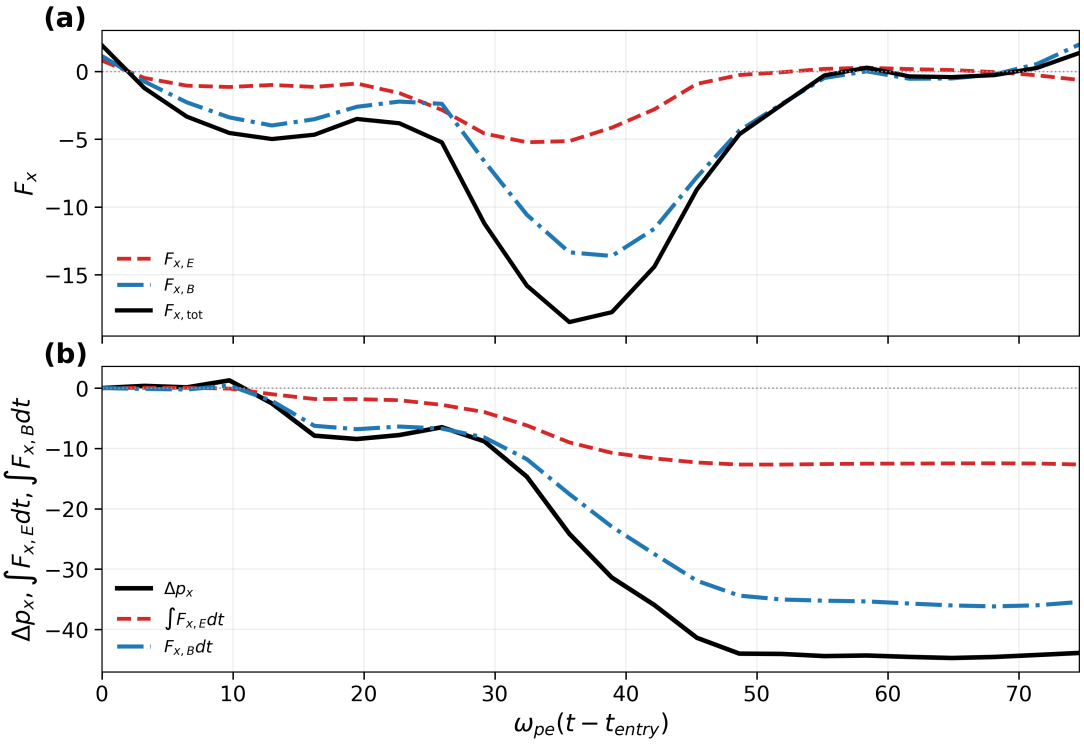


Figure 3. (a) Longitudinal electric contribution to the Lorentz force, ($F_{x,E} = q_i E_x$) (red dashed), magnetic force contribution, ($F_{x,B} = -q_i v_z B_y$) (blue dash-dotted), and total longitudinal force, ($F_{x,\mathrm{tot}} = F_{x,E} + F_{x,B}$) (black), as functions of time measured from MDV entry. The magnetic force contribution dominates during the strongest interaction. (b) Change in longitudinal momentum, (Δp_x (black)), compared with the momentum change due to the electric, ($\int F_{x,E}dt$) (red dashed), and magnetic, ($\int F_{x,B}dt$) (blue dash-dotted), components. The decrease in p_x is governed primarily by the magnetic contribution.

When $\mid v_x - v_{d,x} \mid$ remains large, the ion rapidly drifts through the structure and the interaction terminates. In contrast, when v_x approaches $v_{d,x}$, the ion can remain within the MDV for an extended time. We refer to this condition as phase matching. The different behavior of the two ion Populations is illustrated in Fig. 4(a). For the sample Population I ion, $\mid v_x - v_{d,x} \mid$ decreases rapidly during the MDV interaction and approaches zero at $\omega_{pe}(t - t_{entry}) \simeq 25$. The ion therefore becomes approximately phase matched with the moving MDV and remains within the accelerating region for an extended interval. In contrast, the Population II ion retains a large relative longitudinal velocity and continues to drift through the MDV. This difference in relative motion directly affects the duration of acceleration. As shown in Fig. 4(b), the Population I ion experiences a rapid and sustained increase in energy as its relative velocity approaches zero, reaching $\Delta\gamma_i \simeq 19$. The Population II ion, which does not achieve phase matching, leaves the interaction region earlier and reaches only $\Delta\gamma_i \simeq 5$. Once the interaction terminates, the energy of each ion saturates. The energy evolution satisfies $\Delta\gamma_i = \frac{q_i}{m_i c^2} \int \mathbf{E} \cdot \mathbf{v} dt \simeq \frac{q_i}{m_i c^2} \int E_z v_z dt$, where the second expression follows from the dominance of the transverse electric work demonstrated in Fig. 2(d). Phase matching therefore does not directly provide energy to the ion. Instead, the magnetic Lorentz force identified in Fig. 3 reduces the ion's longitudinal drift relative to the MDV, thereby extending the interval over which the transverse electric field can perform positive work. Figures 4(c-d) shows the same mechanism for all tracked ions. Figure 4(c) shows the averaged longitudinal relative velocity, $< |v_x - v_{d,x}| >$, evaluated across 62 tracked ions from Population I and 62 from Population II. Population I shows a considerable decrease in relative velocity during the interaction, reaching a minimum near the time at which the strongest energization begins. Population II maintains a much larger relative velocity and therefore experiences greater longitudinal drift with respect to the MDV. Correspondingly, Fig. 4(d) shows a much larger mean energy gain for Population I than for Population II. Together, the single-particle and all tracked particle results establish that magnetic-force longitudinal slowing promotes phase matching with the moving MDV, thereby extending the interval over which the transverse electric field can perform positive work which leads to substantial ion energization.

Electric-Field Contributions to Ion Energization

In the previous section, we showed that longer phase matching enables sustained ion energization. We now identify the electric-field components responsible for this energy gain. Since the MDVs propagate mostly along the negative x-direction, towards the downstream with velocity $v_{d,x}$, their motion generates a motional transverse electric field, $E_{z,mot} = -v_{d,x} B_y$. We define the remaining contribution as $E_{z,rem} = E_z - E_{z,mot}$. This component contains inductive electric field produced by the evolution of the MDV together with other local plasma electric fields that are not associated with MDV translational motion. Figure 5 compares these field components for sample Population I and Population II ions. Panels (a) and (b) show the transverse electric field together with its motional and remaining contributions during the interaction with the MDV. In both cases, the motional field reproduces the overall temporal evolution of the field, demonstrating that the propagation of the MDV is responsible for a substantial fraction of the electric field experienced by the ions. Nevertheless, noticeable differences remain during the interval of strongest acceleration, indicating that induced and plasma-generated electric fields also contribute significantly to the interaction. The total work associated with each component is shown in Figs. 5 (c,d). For both ion populations, the work performed by the motional field and the remaining field increases simultaneously throughout the interaction. Their combined contribution closely reproduces the total work obtained directly from the measured transverse electric field, confirming that the decomposition is self-consistent. These results identify the physical mechanism of the accelerating electric field. Both electric field components ($E_{z,mot}, E_{z,rem}$) contribute to ion energization, whereas phase matching is governed by the magnetic component of the Lorentz force, which reduces the ion's longitudinal velocity relative to the MDV. This analysis reveals a clear distinction between the two ion Populations. The Population I ion remains phase matched with the moving MDV for a much longer time and therefore gains considerably more energy from both the motional and remaining electric fields. In contrast, the Population II ion leaves the accelerating region much earlier because of its larger longitudinal relative velocity. As a result, the energy contributions from both components terminate sooner. These results demonstrate that the moving MDV acts as more than a magnetic scattering center. Its propagation generates a strong motional electric field that contributes directly to ion acceleration, while the remaining field, which includes induced and locally generated plasma electric fields, provides a comparable additional contribution. By continuously deflecting the ion trajectory and reducing its longitudinal drift relative to the moving MDV structure, the magnetic field extends the time interval over which the transverse electric field can perform positive work. Ion energization therefore results from the combined action of the motional and induced and plasma-generated electric fields acting during an extended period of phase-matched interaction.

Discussion

The present work demonstrates that upstream MDVs can efficiently pre-accelerate ions and, in some cases, reverse their longitudinal motion, returning them toward the shock transition region with considerably higher energies. These ions therefore can easily feed into shock acceleration processes. An example of repeated upstream interactions is shown in Fig. 6. Figure 6 (a) shows the trajectory of an ion (blue) overlaid on the spatiotemporal evolution of the ion density. Rather than interacting with

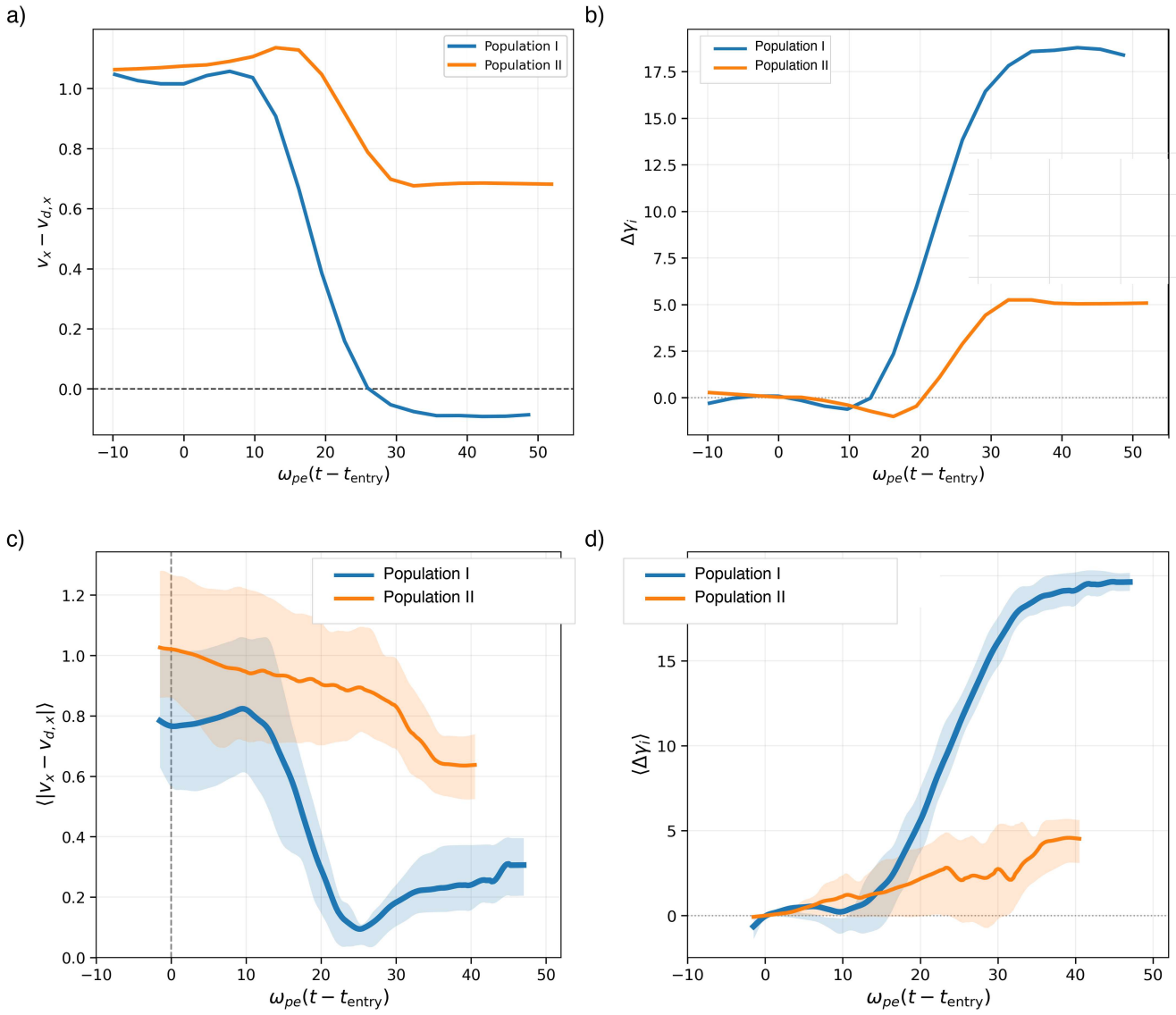


Figure 4. (a) Longitudinal ion velocity relative to MDV, $v_{rel,x}$, for sample Population I and Population II ions. (b) Corresponding ion energy gain, $\Delta\gamma_i$. The Population I ion remains nearly phase matched with MDV for a longer time period and undergoes much larger energization, whereas the Population II ion experiences larger longitudinal drift, exits the interaction region sooner, and gains significantly less energy. (c) Averaged longitudinal relative velocity, $< |v_{rel,x}| >$, for all tracked Population I and Population II ions. Shaded regions indicate the interquartile range. (d) Corresponding averaged energy gain, $< \Delta\gamma_i >$. Together with the single-particle dynamics, the all tracked ions behavior shows that reduced longitudinal velocity relative to the MDV is associated with prolonged interaction and considerably greater ion energization.

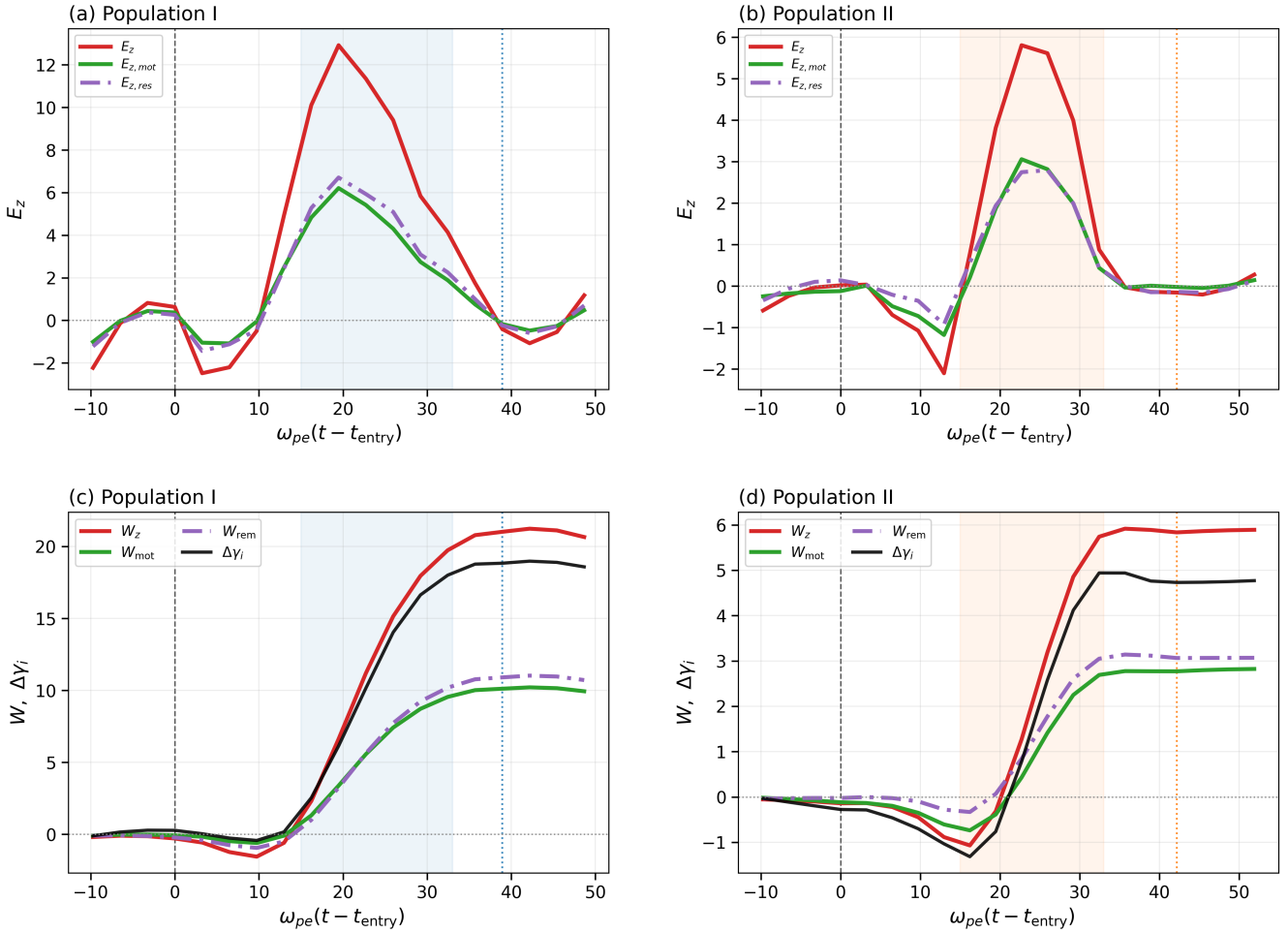


Figure 5. (a,b) Transverse electric field (E_z) (red), motional component ($E_{z,\mathrm{mot}} = -v_d B_y$) (green), and remaining component ($E_{z,\mathrm{rem}} = E_z - E_{z,\mathrm{mot}}$) (purple dash-dotted) experienced by representative Population I and Population II ions, respectively. The shaded regions indicate the interaction intervals inside the MDV. (c,d) transverse work (W_z) performed by the total electric field, together with the contributions from the motional ((W_{mot})) and remaining ((W_{rem})) electric fields, compared with the measured ion energy gain ($\Delta\gamma_i$).

only a single MDV, the ion encounters several MDVs while propagating through the upstream region of the shock before finally returning toward the shock transition region (black curve). The trajectory color denotes the ion energy, illustrating the gradual increase in energy during its upstream evolution. Figure 6(b) shows the corresponding temporal evolution of the ion energy together with the work performed by the longitudinal (W_x) and transverse (W_z) electric fields. The sample ion gains some modest energy during interaction with several upstream MDVs, whereas the final interaction contributes the dominant fraction of the total energy gain. Figures 6(c) and 6(d) further demonstrate that this last interaction is accompanied by a rapid increase in ion energy, a large decrease of the longitudinal momentum, and a simultaneous increase in the transverse momentum, redirecting the ion toward the shock transition region. The upstream region is populated by numerous MDVs generated through the nonlinear evolution of the Weibel instability. These structures continuously propagate toward the shock while simultaneously growing, merging, evolving and dissipating. Consequently, an energetic ion is not limited to interacting with a single MDV. Instead, it may successively interact with several MDVs before eventually reaching the shock transition region. During each interaction, the ion gains a modest amount of energy through the electromagnetic fields. Although the energy gain during an individual interaction is often limited, the total effect of multiple interactions can increase the ion energy before the particle reaches the shock. Our results suggest that the final strong interaction is different from the earlier interactions. During the initial interactions, the ion remains in the upstream region and experiences relatively modest energization, similar to the Population II behavior discussed in this work. In the final interaction, as the ion energy and trajectory evolve, favorable phase matching during a subsequent MDV encounter can significantly increase the interaction time. The resulting extended interaction with the transverse electric field allows considerably more work to be performed on the particle. At the same time, the longitudinal momentum is decreased, eventually reversing the ion motion and returning it toward the shock transition region (Population I behavior discussed in this paper). The final interaction therefore acts not only as the largest energy-gain event but also as the mechanism that redirects the particle back toward the shock. To examine the robustness of the proposed mechanism, we performed an additional simulation with an ion-to-electron mass ratio of $m_i/m_e = 100$. The same physical processes observed for $m_i/m_e = 32$ were also observed at the larger mass ratio. The characteristic ion timescales and energy evolution scale with the ion mass as expected, while the acceleration mechanism remains unchanged. Figure 6 explains the formation of a population of energetic upstream seed ions. Rather than a single acceleration event, these particles may experience a sequence of interactions with MDVs while traversing the upstream. The upstream itself therefore acts as a pre-acceleration region in which ions gain energy before interacting with the shock. By the time they return to the shock transition region, these particles reach the shock transition region with much higher energies than the incoming upstream ions, making them potential seed particles for subsequent shock acceleration. It is important to distinguish this upstream pre-acceleration mechanism from diffusive (Fermi) shock acceleration. The present simulations follow ions only until they return to the shock transition region and therefore do not demonstrate repeated shock crossings or the development of a Fermi acceleration cycle. Instead, our results identify a self-consistent mechanism that prepares ions for those later processes. The repeated interactions with upstream MDVs generate an energetic seed population that may be more readily injected into subsequent shock acceleration with significantly greater efficiency than the original upstream plasma. Following these injected ions through multiple shock crossings would require a much larger computational domain and longer simulation times than those considered here. Such simulations will be the subject of future work. Nevertheless, the mechanism identified in this study establishes upstream MDVs as an important component of particle acceleration in relativistic collisionless shocks. Together with our previous demonstration of upstream electron acceleration by MDVs, the present work suggests that these self-generated electromagnetic structures provide a common pre-acceleration environment for both plasma species, although through distinctly different physical mechanisms. By bridging the thermal upstream plasma and the energetic particles available for later shock acceleration, MDVs may play an important role in determining both the efficiency of particle injection and the resulting nonthermal particle population.

References

1. Piran, T. The physics of gamma-ray bursts. *Rev. Mod. Phys.* **76**, 1143, DOI: https://doi.org/10.1103/RevModPhys.76.1143 (2004).
2. Gehrels, P., N. Meszars. Gamma-ray bursts. *Science* **337**, 932, DOI: 10.1126/science.1216793 (2012).
3. Warren, J. S. *et al.* Cosmic-ray acceleration at the forward shock in tycho's supernova remnant: Evidence from chandra x-ray observations. *Astrophys. J.* **634**, 376, DOI: 10.1086/496941 (2005).
4. Lemoine, M., Gremillet, L., Pelletier, G. & Vanthieghem, A. Physics of weibel-mediated relativistic collisionless shocks. *Phys. Rev. Lett.* **123**, 035101, DOI: 10.1103/PhysRevLett.123.035101 (2019).
5. Weibel, E. Spontaneously growing transverse waves in a plasma due to an anisotropic velocity distribution. *Physicsl Rev. Lett.* **2**, 83–84, DOI: https://doi.org/10.1103/PhysRevLett.2.83 (1959).
6. Medvedev, M. V. & Loeb, A. Generation of magnetic fields in the relativistic shock of gamma-ray burst sources. *Astrophys. J.* **526**, 697, DOI: https://iopscience.iop.org/article/10.1086/308038 (1999).

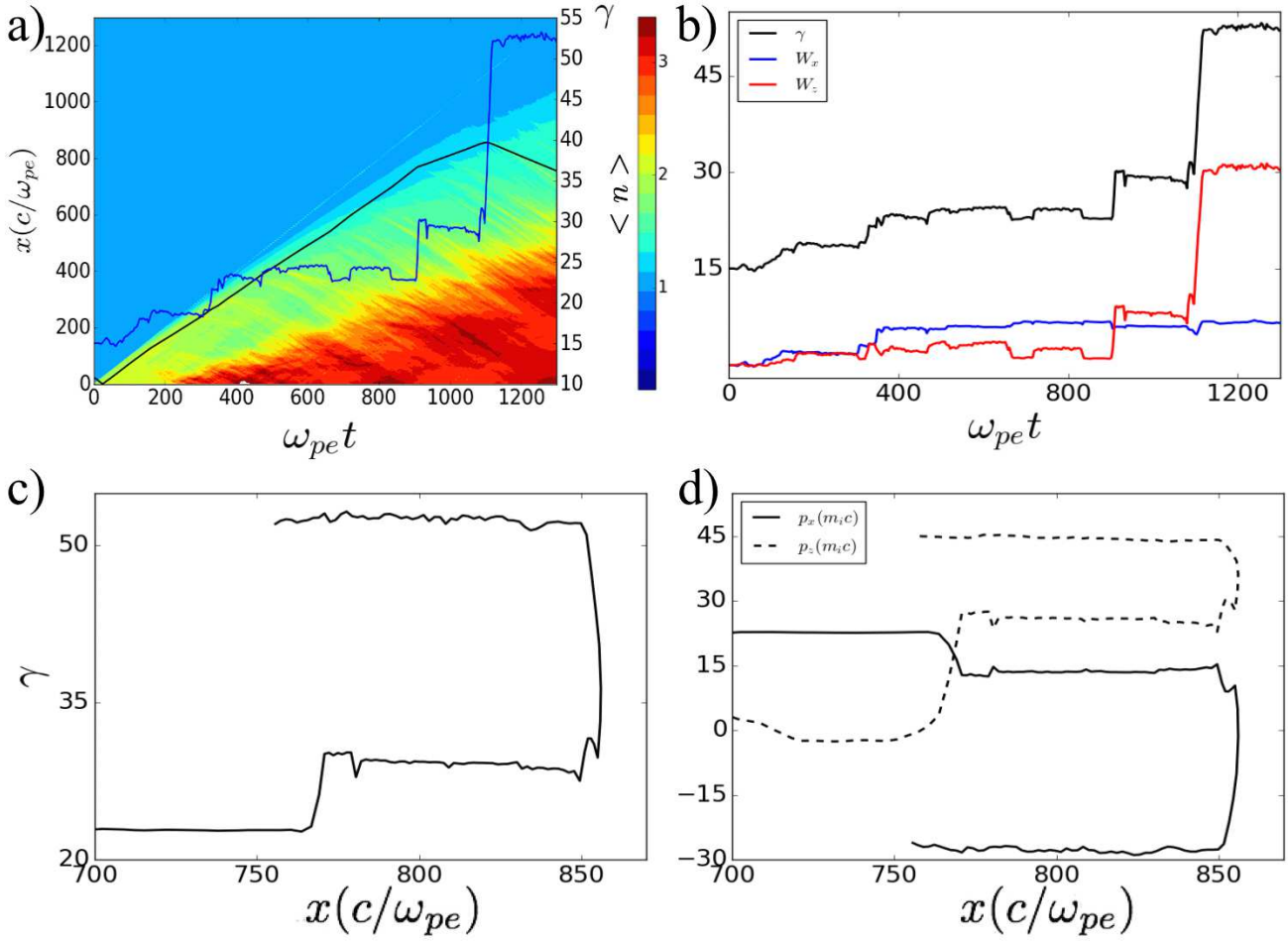


Figure 6. (a) Trajectory of a sample ion (black) and its energy (blue), overlaid on color plot of transversely averaged plasma density in $x-t$ plane. (b) Evolution of the ion energy γ_i and work done by longitudinal (W_x) and transverse (W_z) components of electric field . (c) Ion energy during the final MDV interaction as a function of longitudinal position. (d) Corresponding longitudinal (p_x) and transverse (p_z).

7. Silva, L. O., Fonseca, R. A., Tonge, J. W., Dawson, W. B., J. M. Mori & Medvedev, M. V. Generation of magnetic fields in the relativistic shock of gamma-ray burst sources. *Astrophys. J.* **526**, 697, DOI: https://doi.org/10.1086/308038 (2003).

8. Frederiksen, J., Hededal, C., Haugbølle, T. & Nordlund, A. Magnetic field generation in collisionless shocks: Pattern growth and transport. *The Astrophys. J.* **608**, L13, DOI: https://iopscience.iop.org/article/10.1086/421262 (2004).

9. Medvedev, M., Fiore, M., Fonseca, R. A., Silva, L. O. & Mori, W. B. Long-time evolution of magnetic fields in relativistic gamma-ray burst shocks. *Astrophys. J.* **618**, L75, DOI: https://doi.org/10.1086/427921 (2005).

10. Nishikawa, K., Hardee, P. E., Hededal, C. B. & Fishman, G. J. Particle acceleration, magnetic field generation, and emission in relativistic shocks. *Astrophys. J.* **38**, 1316–1319, DOI: https://doi.org/10.1016/j.asr.2005.01.036 (2006).

11. Spitkovsky, A. On the structure of relativistic collisionless shocks in electron-ion plasmas. *Astrophys. J.* **637**, L39, DOI: 10.1086/527374 (2008).

12. Bret, A. Weibel, two-stream, filamentation, oblique, bell, buneman...which one grows faster? *Astrophys. J.* **699**, 990, DOI: https://doi.org/10.1088/0004-637X/699/2/990 (2009).

13. Stockem Novo, A., Bret, A., Fonseca, R. A. & Silva, L. O. Shock formation in electron–ion plasmas: Mechanism and timing. *Astrophys. J.* **803**, L29–L34, DOI: https://doi.org/10.1088/2041-8205/803/2/L29 (2015).

14. Fiuza, F., Fonseca, R., Tonge, J., Mori, W. & Silva, L. Weibel-instability-mediated collisionless shocks in the laboratory with ultraintense lasers. *Phys. Rev. Lett.* **108**, 235004, DOI: https://journals.aps.org/prl/pdf/10.1103/PhysRevLett.108.235004 (2012).

15. Fiuza, F. & et al. Electron acceleration in laboratory-produced turbulent collisionless shocks. *Nat. Phys.* **16**, 916, DOI: https://doi:10.1038/s41567-020-0919-4 (2020).

16. Huntington, C. & et al. Observation of magnetic field generation via the weibel instability in interpenetrating plasma flows. *Nat. Phys.* **11**, 173, DOI: https://doi:10.1038/NPHYS3178 (2015).

17. Naseri, N. *et al.* Growth and propagation of self-generated magnetic dipole vortices in collisionless shocks produced by interpenetrating plasmas. *Phys. Plasmas* **25**, 012118, DOI: https://doi.org/10.1063/1.5008278 (2018).

18. Spitkovsky, A. Particle acceleration in relativistic collisionless shocks: Fermi process at last? *The Astrophys. J.* **682**, L5, DOI: 10.1086/590248 (2008).

19. Kato, T. N. & Takabe, H. Nonrelativistic collisionless shocks in unmagnetized electron-ion plasmas. *The Astrophys. J.* **681**, L93, DOI: 10.1086/590387 (2008).

20. Peterson, J. R., Glenzer, S. & Fiuza, F. Magnetic field amplification by a plasma cavitation instability in relativistic shock precursors. *The Astrophys. J. Lett.* **924**, L12, DOI: 10.3847/2041-8213/ac44a2 (2022).

21. Naseri, N., Bochkarev, S. G., Bychenkov, V. Y. *et al.* Electron energization dynamics in interaction of self-generated magnetic vortices in upstream of collisionless electron/ion shocks. *Sci Rep* **12**, 7327, DOI: https://doi.org/10.1038/s41598-022-11163-2 (2022).

22. Sironi, L. & Spitkovsky, A. Particle acceleration in relativistic magnetized collisionless electron–ion shocks. *The Astrophys. J.* **726**, 75, DOI: 10.1088/0004-637X/726/2/75 (2010).

23. Vanthieghem, A. *et al.* Electron heating in high mach number collisionless shocks. *Phys. Rev. Lett.* **132**, 265201, DOI: 10.1103/PhysRevLett.132.265201 (2024).

24. Martins, S. F., Fonseca, R. A., Silva, L. O. & Mori, W. B. Ion dynamics and acceleration in relativistic shocks). *Astrophys. J.* **695**, L189, DOI: https://doi:10.1088/0004-637X/695/2/L189 (2009).

25. Pukhov, A. Three-dimensional electromagnetic relativistic particle-in-cell code vlpl (virtual laser plasma lab). *J. Plasma Phys.* **61**, 425, DOI: https://doi.org/10.1017/S0022377899007515 (1999).

26. Bret, A. *et al.* Collisionless shock formation, spontaneous electromagnetic fluctuations, and streaming instabilities plasma). *Phys. Plasmas* **20**, 042102, DOI: https://doi.org/10.1063/1.4798541 (2013).

27. Yadav, S. & Das, A. Nonlinear studies of fast electron current pulse propagation in a two dimensional inhomogeneous plasma). *Phys. Plasmas* **17**, 052306, DOI: https://doi.org/10.1063/1.3407621 (2010).

28. Gedalin, M. Linear waves in relativistic anisotropic magnetohydrodynamics). *Phys. Rev. E* **47**, 4354, DOI: https://doi.org/10.1103/PhysRevE.47.4354 (1993).

Data availability

The datasets generated and analyzed during the current study are not publicly available due to the large size of the raw particle-in-cell simulation output files but are available from the corresponding author on reasonable request.

Funding

This work was supported by Adelphi Faculty Development Grant.

Acknowledgements

The authors wish to thank Texas Advanced Computing Center and ACCESS for providing computational resources and their help to restore our simulation data.

Author contributions statement

N. Naseri performed simulations, analyzed results, generated figures and prepared manuscript. N. Naseri, and G. Shvets discussed the results. All authors reviewed the manuscript.

Supplementary Files

This is a list of supplementary files associated with this preprint. Click to download.

- poulationIsingleionenergymovie.mp4
- populationIIsingleionenergymovie.mp4